Proceedings of the 21st ICSMGE, Vienna, Austria, 14 – 19 June 2026. Pistrol, Adam & Schweiger (eds.)
Published by: ÖGG, Austrian Society for Geomechanics, Salzburg, Austria, ISBN 978-3-9503898-4-5
https://doi.org/10.53243/ICSMGE2026-1103

Understanding soil liquefaction potential in Lebanon based on non-linear modeling

Hiba Labaki
Civil and Environmental Engineering department, Saint Joseph University of Beirut, Beirut, Lebanon
National Center for Geophysics, National Council for Scientific Research, Beirut, Lebanon, hiba.labaki@net.usj.edu.lb

Muhsin Elie Rahhal
Civil and Environmental Engineering department, Saint Joseph University of Beirut, Beirut, Lebanon

Marleine Brax
National Center for Geophysics, National Council for Scientific Research, Beirut, Lebanon

Etienne Bertrand, Luis Fabian Bonilla
IPGP, Paris Cité University, Paris, France
GERS-SRO, Gustave Eiffel University, Champs-sur-Marne, France

ABSTRACT: This study presents a site-specific analysis of soil non-linearity and liquefaction susceptibility in northeastern Beirut, Lebanon, using 1D non-linear simulations. The liquefaction front model of Iai et al. (1990) is employed to simulate pore pressure generation and dilatant soil behavior under cyclic loading. The model dilatancy parameters are estimated through inversion of empirical Liquefaction Resistance Curves using the Neighborhood algorithm (Sambridge, 1999). Multiple sets of dilatancy parameters with acceptable misfits are tested to evaluate their influence on non-linear soil response and liquefaction potential under various strong motion scenarios. Results highlight the importance of accounting for variations in dilatancy parameters, the duration and frequency content of the seismic input. The proposed approach offers a reliable framework for improving seismic hazard assessment in Lebanon.

KEYWORDS: Liquefaction susceptibility, cyclic mobility, 1D non-linear numerical modeling, seismic hazard, Lebanon.

1 INTRODUCTION

Soil liquefaction is a phenomenon that can cause serious damage to buildings and infrastructure during earthquakes. Under strong shaking, saturated granular soils can exhibit complex responses, such as shear stiffness degradation and an increase of energy dissipation, that are strongly dependent on strain levels (Beresnev & Wen 1996; Bonilla et al. 2005; Roten et al. 2009). To assess these complexities, advanced numerical modeling is necessary. These assessments are particularly relevant for Beirut, which, despite its current low seismicity, has a historical record of destructive earthquakes (Brax et al. 2019). The presence of shallow groundwater tables and unconsolidated Quaternary deposits creates conditions that are highly susceptible to liquefaction (Rahhal, 2008) and non-linear soil behavior. Given the city's dense urbanization, accurately characterizing site-specific soil response and liquefaction potential under seismic loading is essential for improving seismic hazard assessment.

In a previous study, Labaki et al. (2025) used the finite-difference code NOAH (NOn-linear Anelastic Hysteretic) to perform 1D non-linear simulations of soil behavior (Bonilla, 2001). NOAH includes the multishear mechanism model to reproduce hysteretic stress-strain behavior (Towhata & Ishihara 1985), and the liquefaction front model to simulate the cyclic mobility of cohesionless soils (Iai et al. 1990) at a site in the eastern suburbs of Beirut, Lebanon. The liquefaction front model depends on five dilatancy parameters that control pore pressure development, which can be obtained from laboratory data. However, in the absence of such data, Standard Penetration Test (SPT) results were used to invert empirical Liquefaction Resistance Curves (LRC) as proposed by Janusz et al. (2024). To do so, an inversion technique using the Neighborhood Algorithm (Sambridge, 1999) was applied, based on deterministic methods (Boulanger & Idriss 2014), derived from existing SPT data, to estimate the dilatancy parameters. Building on this approach, this paper explores various sets of dilatancy parameters derived from the inversion under different earthquake ground motions.

In this study, the emphasis is placed on the phenomenon of cyclic mobility rather than flow liquefaction, as the investigated soils are predominantly medium-dense sands, which exhibit dilative behavior under cyclic loading. Cyclic mobility refers to the progressive buildup of pore water pressure during cyclic loading, leading to temporary reductions in shear strength and incremental shear deformations, while the soil retains some strength between cycles. This behavior is typical of medium to dense cohesionless soils, in contrast to the sudden and complete loss of strength observed in flow liquefaction of loose sands (Castro & Poulos 1977; Elgamal et al. 2003).

The main objective is to investigate how variations in input parameters and shaking levels influence soil non-linearity and cyclic mobility, and to identify the characteristics that most significantly affect the response.

In the following sections, the methodology is presented, followed by the simulations results. Afterwards, the implications of these findings for assessing the liquefaction hazard in Beirut are discussed.

2 CASE STUDY

Labaki et al. (2025) identified a site located in the eastern suburbs of Beirut, near the Beirut River, to study the cyclic mobility of the soil. Geologically, the site is made up of Quaternary sandy alluvium resting on older Cretaceous formations. These Quaternary deposits, approximately 45 meters thick, consist of various unconsolidated soils overlying the bedrock. The groundwater table is shallow, located at a

depth of around 2 meters, roughly corresponding to the local sea level.

SPT were carried out at 1.5 m intervals. The soil profile shown in Figure 1, is divided into four main layers: fill (0–2 m), sand (2–16.5 m), sandy clay (16.5–28 m), and a deeper sand layer (28–45 m). Based on the SPT results, five sandy layers, primarily located above 15 meters, were identified as potentially liquefiable due to their low blow counts (Sebaaly, 2022). This analysis follows the conceptual framework of Labaki et al. (2025) to assess the non-linear behavior of soils and their liquefaction potential. During the inversion process, optimal dilatancy parameters were identified by minimizing the misfit that is defined as the squared difference between modeled empirical LRC and the observed LRC. In the present study, using the same site and modeling approach as Labaki et al. (2025), the analysis is expanded to explore the influence of dilatancy parameter sets corresponding not only to the minimum but also to acceptable misfit values below 0.3.

Additionally, two different input motions are incorporated to explore the variability of soil response across a range of seismic scenarios, including variations in duration.

3 METHODOLOGY

3.1 *Data selection*

To explore the influence of model parameter variability, multiple dilatancy parameter sets were considered for each liquefiable layer. In addition to the minimum misfit set found in a previous study (Labaki et al. 2025), three alternative sets of dilatancy parameters with acceptable misfit values were identified for Layer 2. Similarly, for Layers 4, 5, and 6, two additional acceptable sets were selected for each, and for Layer 7, one additional set was included alongside the minimum misfit set. Examples of the dilatancy parameter sets used for layer 2 are presented in Table 1.

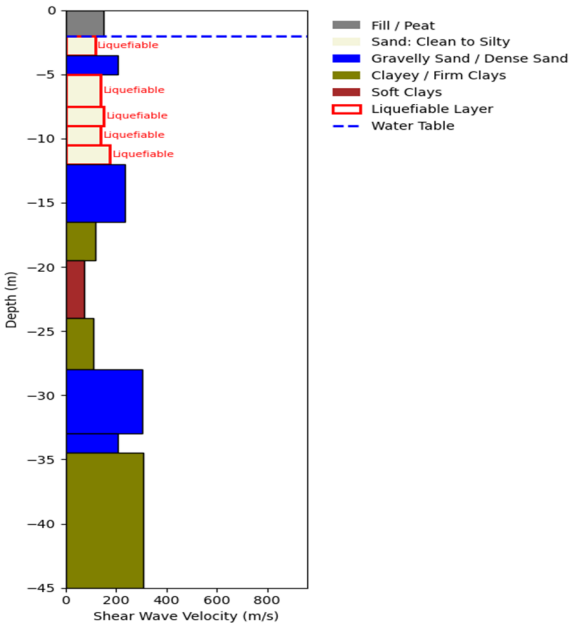

Figure 1. Soil profile divided into layers with corresponding shear wave velocity values.

To study how the dilatancy parameters affect the soil resistance to cyclic loading, we plotted the Cyclic Stress Ratio (CSR) versus the number of cycles (N), as shown in Figure 2. The CSR is defined as the ratio of cyclic shear stress (τ) to the initial mean effective stress (σ'_{m0}). These plots help visualize the Liquefaction Resistance Curves (LRCs), which represent the number of loading cycles required to induce liquefaction at a given CSR. The LRCs obtained from the inversion are shown in color and are classified by their misfit values, while empirical LRCs are shown in black with circular markers. The CSR–N curve serves as a common link between the four dilatancy parameter sets, allowing for a direct comparison of their effects. A total of 51 parameter combinations were generated by systematically varying the dilatancy sets across the five liquefiable layers. Each combination involved assigning one specific set of dilatancy parameters to each layer and the NOAH code was used to simulate the resulting non-linear soil behavior. An illustration of four representative combinations is provided in Table 2.

To assess the sensitivity of soil response to seismic loading, each of the 51 parameter combinations was tested under two input motions, whose characteristics are summarized in Table 3 and illustrated in the acceleration–time plots of Figure 3.

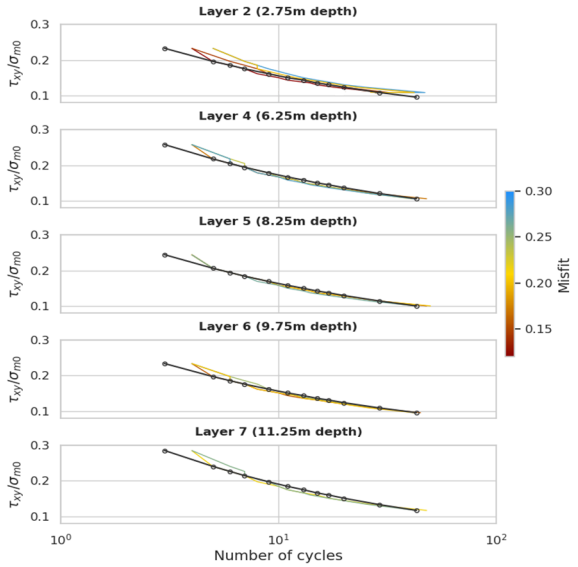

Figure 2. Liquefaction Resistance Curve (LRC) obtained from the SPT test for all five liquefiable layers (represented by circular markers) compared to LRCs of the sets of dilatancy parameters, with misfit indicated by color.

The two ground motions, AB089 and SM502, were selected from the European Strong Motion (ESM) database due to their contrasting characteristics and relevance to regional seismic hazard. AB089 corresponds to the 1999 Chi-Chi earthquake in Taiwan (Mw = 7.7), while SM502 was recorded during the 2000 Island earthquake (Mw = 6.5). AB089 features a relatively long duration of about 40 seconds and a lower peak ground acceleration (PGA) of 0.35 g, whereas SM502 has a shorter duration of approximately 20 seconds but a higher PGA of 0.529 g. Both motions were recorded on sites classified as type A in the ESM database. Spectral analysis of the two signals (Figure 4), using the Konno and Ohmachi (1998) smoothing algorithm with a bandwidth of 40, shows that both inputs exhibit a predominant frequency around 3 Hz. However,

AB089 presents slightly higher spectral amplitudes extending up to 10 Hz, thus having a larger frequency bandwidth.

Their selection was based on the seismic hazard in Lebanon. The two records align with the deterministic scenario adopted for the 551 AD earthquake in Beirut, as outlined in the seismic hazard assessment for the Beirut Urban Resilience Master Plan (Brax et al. 2020). This historical earthquake is modeled with a magnitude Mw = 7.3 and a fault rupture located directly beneath the city along the Mount Lebanon Thrust fault. The expected PGA values for this scenario range from 0.30 g to 0.55 g, which fall within the range covered by AB089 and SM502. Accordingly, these two input motions were used in the simulations to investigate the linear and non-linear site response at the Beirut site. As demonstrated by Labaki et al. (2025), though not shown here, linear simulations under the two input motions at the Beirut site revealed that the fundamental frequency is at around 0.9 Hz. This result is consistent with findings reported by Brax et al. (2018) and Safa (2025). For the non-linear case under SM502, we observe a typical non-linear behavior characterized by a shift of the fundamental frequency toward 0.5 Hz, the appearance of an additional peak around 1 Hz due to cyclic mobility, and attenuation at high frequencies.

Table 1. Dilatancy parameter sets with minimum and acceptable misfit values for liquefiable layer 2.

Parameter	Set with the Minimum Misfit	Set 1	Set 2	Set 3
p_1	0.564	0.742	0.920	0.423
p_2	1.936	1.582	1.002	1.053
c_1	2.003	1.907	2.138	2.026
w_1	3.960	4.145	2.394	2.372

Table 2. Example of five combinations.

Combinations	Layer 2	Layer 4	Layer 5	Layer 6	Layer 7
Combination_3	Set 2	Set 1	Set 2	Set 1	Set 1
Combination_12	Set with Min misfit	Set with Min misfit	Set 1	Set with Min misfit	Set with Min misfit
Combination_17	Set 1	Set with Min misfit	Set with Min misfit	Set with Min misfit	Set with Min misfit
Combination_34	Set 2	Set with Min misfit	Set 2	Set 1	Set with Min misfit

Table 3. Characteristics of the ground motions used in the numerical simulations.

Event	Taiwan	Island
Network	A	SM
Station	B089	502
Date	20-Sep-1999	17-Jun-2000
Mw	7.7	6.5
amax (g)	0.35	0.529
Component	N	N
Epicentral Distance (km)	19.5	8.4
Soil Deposit	A	A
Database	ESM (Engineering Strong Motion)	ESM (Engineering Strong Motion)

3.2 *Threshold criteria for cyclic mobility*

This study compares different output parameters, including maximum shear strain, duration of the signal, acceleration at the surface and excess pore water pressure. Cyclic mobility is considered to have occurred when both the pore pressure ratio (ru) exceeds 0.9 and the single-amplitude axial strain exceeds 2.5% (or 5% double amplitude), (Ishihara, 1993; Rahhal & Lefebvre 2000). These two thresholds are indicated by orange dashed lines in Figures 5 and 8 to clearly mark the limits. For visual clarity, the plots display the minimum and maximum values among the 51 simulation combinations and are limited to a depth of 20 meters, although the full soil profile extends to 45 meters.

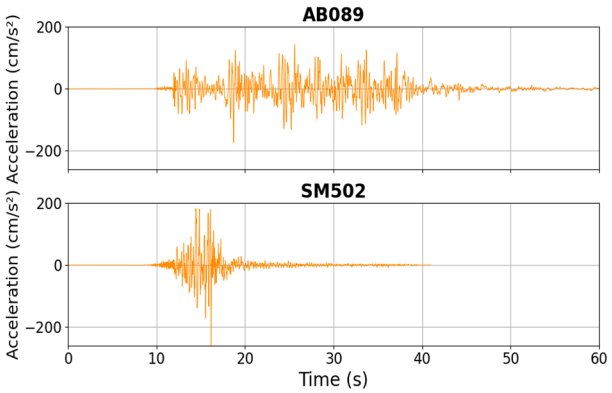

Figure 3. Accelerograms of the two input motions are plotted with a common time axis to better visualize and compare the duration of each seismic recording.

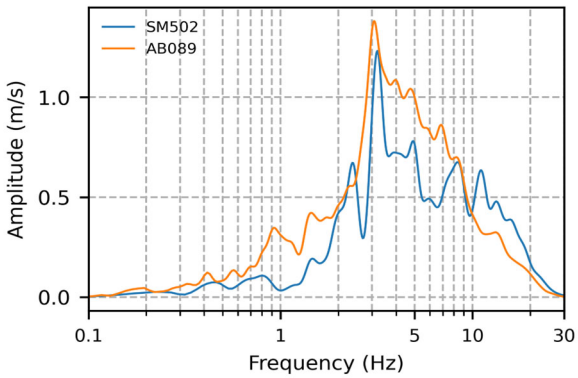

Figure 4. Fourier amplitude spectra of the two selected input accelerograms.

In addition, plotting surface acceleration in non-linear models highlights how the computed ground shaking differs from the input seismic motion due to the complex behavior of the soil. To further illustrate this non-linearity and assess variability across simulations, acceleration time histories at the surface for the minimum and maximum response cases are presented in Figures 6 and 9.

To complement this analysis and gain insight into the development of excess pore pressure and its role in triggering cyclic mobility, the pore pressure ratio versus time is also plotted for the minimum and maximum simulation

combinations under each input motion, as shown in Figures 7 and 10. Comparing the excess pore water pressure (PWP) generated by the two different seismic inputs highlights how motion characteristics influence the buildup of pore pressure. These assessments help evaluate the sensitivity of the soil response to different ground motions and identify which shaking scenarios are more likely to induce cyclic mobility.

4 RESULTS

4.1 *Results for input motion AB089*

The AB089 input motion consistently triggered strong cyclic mobility response across all 51 tested parameter combinations. Layers 2, 4, and 6 were the most affected, where both the pore pressure ratio (ru) exceeded 0.9 and the single-amplitude axial strain surpassed 2.5%, satisfying the dual cyclic mobility criteria (Figure 5). While layer 5 showed high ru, its lower strain levels implied partial susceptibility. Layer 7 remained unaffected in all simulations. The similarity in surface acceleration responses across combinations (Figure 6) indicates that changes in dilatancy parameters had little impact on the motion observed at the surface. However, these changes significantly affected how the soil responded internally, in terms of strain accumulation in layer 2.

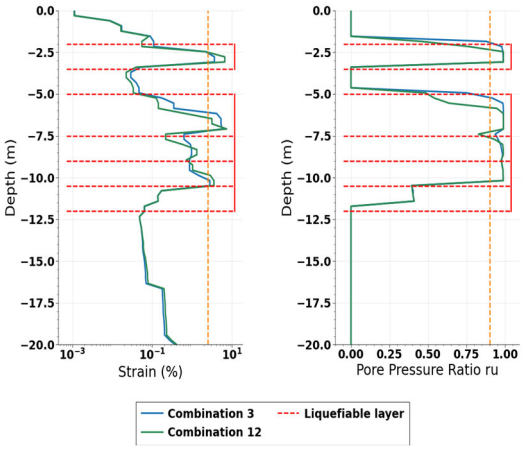

Figure 5. Strain and pore pressure ratio profile for two combinations for the input motion AB089.

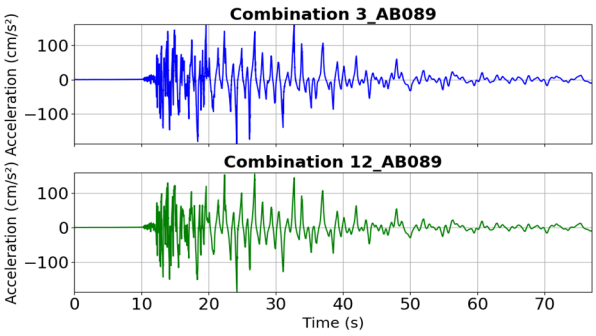

Figure 6. Acceleration vs. time plots at the surface for two combinations for the input motion AB089.

As shown in Figure 7, the pore water pressure buildup curves exhibit minor differences between the two combinations. The dilatancy parameters describe the geometrical shape of the pore pressure evolution curve. In this case, the variability introduced in these parameters had a limited influence on the resulting pore water pressure response.

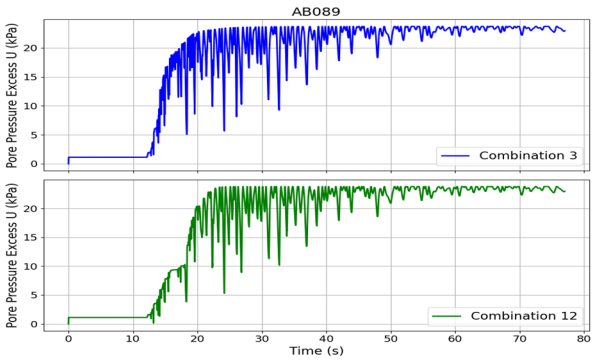

Figure 7. Excess pore water pressure vs. time plots at layer 2 for two combinations for the input motion AB089.

4.2 *Results for input motion SM502*

For SM502, the simulations revealed significant pore pressure buildup in layers 2 and 4 (Figure 8); however, strains generally did not exceed 2.5%, particularly in layers 4 through 7. The limited strain despite high ru underscores the importance of strain-based criteria in accurately identifying liquefaction potential. The marginal cyclic mobility observed in layer 2 emphasizes its unique sensitivity compared to deeper layers. The surface motion (Figure 9) showed little variation across parameter sets, indicating that while changes in dilatancy parameters had minimal effect on surface acceleration, they influenced the internal soil response in terms of strain accumulation in layer 2. In Figure 10, the pore water pressure buildup curves exhibit minor differences between the two combinations, following the same trend observed under the AB089 input in Figure 7.

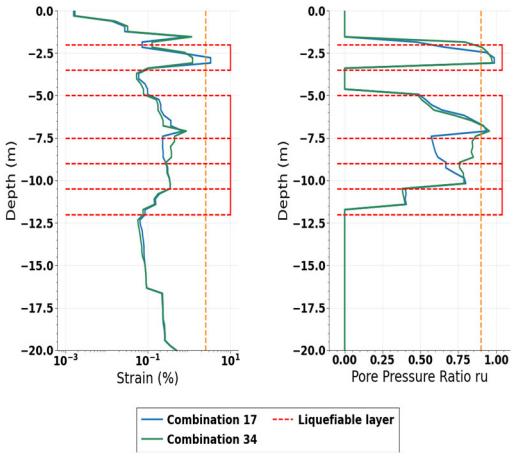

Figure 8. Strain and pore pressure ratio profile for two combinations for the input motion SM502.

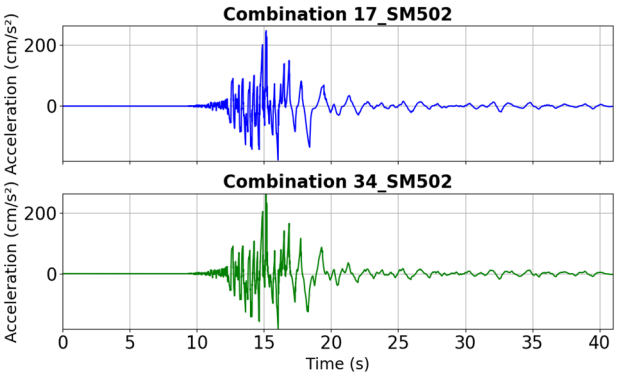

Figure 9. Acceleration vs. time plots at the surface for two combinations for the input motion SM502.

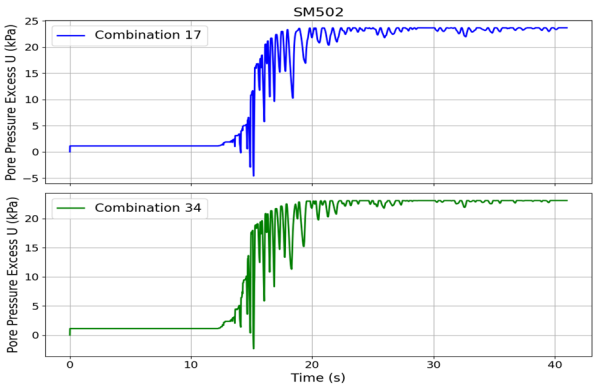

Figure 10. Excess pore water pressure vs. time plots at layer 2 for two combinations for the input motion SM502.

5 ANALYSIS AND DISCUSSION

For the two input motions, layer 2 consistently demonstrated the highest susceptibility to cyclic mobility, with both pore pressure and strain thresholds regularly exceeded.

In Figure 11, the upper panel corresponding to Combination 3 under the AB089 motion exhibits pronounced hysteresis loops and large strain amplitudes, indicating strong non-linear behavior and cyclic mobility. In contrast, the lower panel (Combination 17 under SM502) shows a clearly lower level of non-linearity, with narrower loops and reduced strain. This contrast highlights the significant influence of shaking duration on strain development, even when excess pore pressure levels (ru) are similarly high, as the longer duration of AB089 induces more loading cycles, thereby allowing greater strain accumulation.

While some variability was observed among the 51 parameter combinations, the overall pattern of cyclic mobility occurrence remained stable. Figure 2 illustrates that even when the Cyclic Stress Ratio (CSR)–N curves vary slightly among dilatancy sets, their practical implications in the simulations were often similar, except for the strain values of the layer 2 which is the most non-linear case. It is interesting to study later on, how different sets of dilatancy parameters affect strain, and how modifying one set in a given layer influences the response of the other layers.

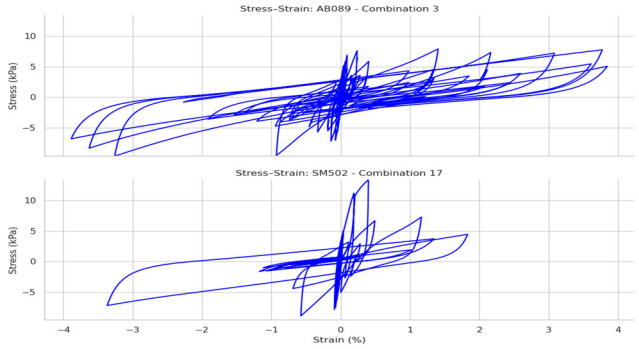

Figure 11. Stress–strain plots at Layer 2: the upper plot corresponds to Combination 3 under input motion AB089, and the lower plot to Combination 17 under input motion SM502.

As for the input motions considered, shaking duration had a greater impact on triggering cyclic mobility than peak ground acceleration (PGA) alone (Figure 3, Table 3). For example, AB089, with its longer duration, led to earlier and more consistent pore pressure buildup than SM502, despite the latter's higher PGA (0.529 g vs. 0.35 g). This reinforces the notion that the duration of strong ground motion plays a critical role in earthquake-induced soil response, as shorter events may lack sufficient load cycles to induce significant strain accumulation, even when their amplitudes are high (Kramer, 1996).

In addition to motion characteristics, it is important to note the contribution of site effects, particularly the basin effect, in shaping ground motion. In sedimentary basins, seismic waves can become trapped and reverberate within deep, soft, sediment-filled valleys, causing a significant amplification of ground motion and prolonged shaking duration (Graves et al. 1998). This behavior was further confirmed by Safa (2025), which investigated 3D site effects in the same basin examined in this study, highlighting how basin geometry significantly influences seismic response. Pore pressure plots (Figures 7 and 10) confirm this, with AB089 producing faster and more sustained increases due to its higher number of stress cycles, ultimately promoting cyclic mobility.

Regarding the correlation between the occurrence of cyclic mobility and the frequency content of the input motions, both AB089 and SM502 exhibit similar frequency characteristics. Therefore, to better understand the potential influence of frequency content, future studies should examine a wider range of seismic signals with varying spectral properties.

Finally, it is important to emphasize that, this study focuses on exploring the cyclic mobility behavior rather than the soil model itself.

6 CONCLUSIONS

This study focuses on the understanding of liquefaction susceptibility in Lebanon by integrating inversion techniques with non-linear soil modeling. By exploring how variations in dilatancy parameters influence soil response under different seismic inputs, a practical tool for regions with limited field and laboratory data is proposed.

The results show that layer 2, composed of shallow sandy soils near the water table, consistently exhibits the highest

susceptibility to cyclic mobility. Across all simulations, the influence of dilatancy parameters on pore pressure buildup was minor but detectable, while their impact on strain development, particularly under marginal cyclic mobility conditions, should be studied more closely in the future.

A key finding of this study is that the duration of shaking and the number of loading cycles are more decisive in triggering cyclic mobility than peak ground acceleration (PGA) alone.

These findings suggest that future studies should select ground motions with broader frequency content to better understand how frequency content interacts with soil behavior and affects the triggering of cyclic mobility.

Finally, the proposed method allows studying site response analysis and enables a seismic hazard assessment in the absence of field and laboratory data. This is the case of countries with low to moderate seismic hazard (Janusz et al. 2024) and regions with a limited seismic network deployment as in Lebanon.

7 REFERENCES

Beresnev, I. A., and Wen, K.-L. 1996. Nonlinear soil response—A reality? *Bulletin of the Seismological Society of America*, 86(6), 1964–1978.

Bonilla, L. F. 2001. *NOAH: User's Manual*. Institute for Crustal Studies, University of California, Santa Barbara, USA; Institut de Radioprotection et de Sûreté Nucléaire, France.

Bonilla, L. F., Archuleta, R., and Lavallée, D. 2005. Hysteretic and dilatant behavior of cohesionless soils and their effects on non-linear site response: Field data observations and modeling. *Bulletin of the Seismological Society of America*, 95, 2373–2395.

Boulanger, R. W., and Idriss, I. M. 2014. *CPT and SPT based liquefaction triggering procedures*. Davis: Center for Geotechnical Modeling, University of California.

Brax, M., Bard, P.-Y., Duval, A.-M., Bertrand, E., Rahhal, M.-E., Jomaa, R., Cornou, C., Voisin, C., and Sursock, A. 2018. Towards a microzonation of the Greater Beirut area: an instrumental approach combining earthquake and ambient vibration recordings. *Bulletin of Earthquake Engineering,* 16, 5735–5767.

Brax, M., Albini, P., Beauval, C., Jomaa, R., and Sursock, A. 2019. An earthquake catalog for the Lebanese region. *Seismological Research Letters*, 90(6), 2236–2249.

Brax, M., Labaki, H., and Bard, P.-Y. 2020. *Beirut Urban Resilience Master Plan (Phase II) Data Scoping; Seismic, and Tsunami Hazard Assessments: Deliverable 6 Spectral Accelerations Per Zone: Deterministic Approach*. National Council for Scientific Research. Report submitted to the World Bank.

Castro, G., and Poulos, S. J. 1977. Factors affecting liquefaction and cyclic mobility. *Journal of Geotechnical Engineering Division, ASCE*, 103(GT6), 501–516.

Elgamal, A., Yang, Z., Parra, E., and Ragheb, A. 2003. Modeling of cyclic mobility in saturated cohesionless soils. *International Journal of Plasticity*, 19, 883–905.

Graves, R. W., Pitarka, A., and Somerville, P. G. 1998. Ground-motion amplification in the Santa Monica area: Effects of shallow basin-edge structure. *Bulletin of the Seismological Society of America*, 88, 1224–124.

Iai, S., Matsunaga, Y., and Kameoka, T. 1990. Parameter identification for a cyclic mobility model. *Report of the Port and Harbour Research Institute*, 29(4), 57–183.

Ishihara, K. 1993. Liquefaction and flow failure during earthquakes. *Géotechnique*, 43(3), 351–415.

Janusz, P., Bergamo, P., Bonilla, L. F., Panzera, F., Roten, D., Loviknes, K., and Fäh, D. 2024. Multistep procedure for estimating non-linear soil response in low seismicity areas—a case study of Lucerne, Switzerland. *Geophysical Journal International*, 239(2), 1133–1154.

Konno, K., and Ohmachi, T. 1998. Ground-motion characteristics estimated from spectral ratio between horizontal and vertical components of microtremor. *Bulletin of the Seismological Society of America*, 88(1), 228–241.

Kramer, S. L. 1996. *Geotechnical Earthquake Engineering*. Upper Saddle River, NJ: Prentice Hall.

Labaki, H., Bertrand, E., Bonilla, L. F., Brax, M., and Rahhal, M. E. 2025. Non-linear soil behavior and liquefaction susceptibility in Lebanon: A 1D numerical approach. In *Proceedings of the 10th International Conference on Computational Methods in Structural Dynamics and Earthquake Engineering (COMPDYN 2025)* (Paper C25652). Rhodes, Greece, 15–18 June 2025.

Rahhal, M. E., and Lefebvre, G. 2000. Understanding the effect of static driving shear stress on the liquefaction resistance of medium dense sand. *Soil Dynamics and Earthquake Engineering*, 8, 397–404.

Rahhal, M. E. 2008. Comprendre les méthodes d'évaluation du potentiel de liquéfaction des sols. Proceedings, *4th Canadian Conference on Geohazards,* Presse de l'Université Laval, Québec, CANADA, 117–124.

Roten, D., Fäh, D., Bonilla, L. F., Alvarez-Rubio, S., Weber, T. M., and Laue, J. 2009. Estimation of non-linear site response in a deep Alpine valley. *Geophysical Journal International*, 178(3), 1597–1613.

Safa, M. 2025. Modélisation numérique des effets de site sismiques induits par la structure 3D superficielle et les hétérogénéités aléatoires des sols : application au Grand Beyrouth. [Doctoral thesis, Université Gustave Eiffel].

Sambridge, M. 1999. Geophysical inversion with a neighbourhood algorithm—I. Searching a parameter space. *Geophysical Journal International*, 138(2), 479–494.

Sebaaly, G. 2022. New insights in the understanding of the hazard mapping of the soil liquefaction potential. [Doctoral thesis, Saint Joseph University of Beirut, Faculty of Engineering – ESIB].

Towhata, I., and Ishihara, K. 1985. Modeling soil behavior under principal axes rotation. In *Proceedings of the 5th International Conference on Numerical Methods in Geomechanics*, 523–530.